JOURNAL OF SPACECRAFT AND ROCKETS
Vol. 44, No. 2, March–April 2007

Mars Exploration Entry, Descent, and Landing Challenges

Robert D. Braun*
Georgia Institute of Technology, Atlanta, Georgia 30332-0150
and
Robert M. Manning†
Jet Propulsion Laboratory, California Institute of Technology, Pasadena, California 91109

DOI: 10.2514/1.25116

The United States has successfully landed five robotic systems on the surface of Mars. These systems all had landed masses below 0.6 metric tons, had landed footprints on the order of hundreds of kilometers, and landed at sites below −1.4 kilometers elevation due the need to perform entry, descent, and landing operations in an environment with sufficient atmospheric density. At present, robotic exploration systems engineers are struggling with the challenges of increasing landed mass capability to 0.8 metric tons while improving landed accuracy to 10 kilometers and landing at a site as high as +2 kilometers elevation for the Mars science laboratory project. Meanwhile, current plans for human exploration of Mars call for the landing of 40–80 metric tons surface elements at scientifically interesting locations within close proximity (tens of meters) of pre-positioned robotic assets. This paper summarizes past successful entry, descent, and landing systems and approaches being developed by the robotic Mars exploration program to increase landed performance (mass, accuracy, and surface elevation). In addition, the entry, descent, and landing sequence for a human exploration system will be reviewed, highlighting the technology and systems advances required.

Nomenclature

A	=	aerodynamic reference area, m^2
C_D	=	aerodynamic drag coefficient
C_L	=	aerodynamic lift coefficient
g	=	one Earth deceleration unit, 9.806 m/s^2
I_{sp}	=	specific impulse, s
L/D	=	lift-to-drag ratio
m	=	mass, kg
α	=	angle of attack, deg
β	=	ballistic coefficient, kg/m^2
ΔV	=	propulsive velocity change, m/s
τ	=	atmospheric opacity

I. Introduction

THE United States has successfully landed five robotic systems on the surface of Mars. These systems all had landed masses below 0.6 metric tons (t), had landed footprints on the order of hundreds of kilometers, and landed at sites below −1.4 km Mars orbiter laser altimeter (MOLA) elevation due to the need to perform entry, descent, and landing operations in an environment with sufficient atmospheric density [1].

Today, robotic exploration systems engineers are struggling with the challenges of increasing landed mass capability to 0.8 t, while improving 3-σ landed accuracy to 10 km, and landing at a site as high as +2 km MOLA elevation for the Mars science laboratory project [2,3]. Subsequent robotic exploration missions under consideration for the 2010 decade, e.g., Mars sample return and astrobiology field laboratory, may require a doubling of this landed mass capability. To date, no credible Mars entry, descent, and landing (EDL) architecture has been put forward that can safely place a 2 t payload at high elevations on the surface of Mars at close proximity to scientifically interesting terrain. This difficulty is largely due to the Mars program's continued reliance on Viking-era space qualification technology, which is reaching its limits.

In contrast, current plans for human exploration of Mars call for the landing of 40–80 t surface elements at scientifically interesting locations within close proximity (tens of m) of pre-positioned robotic assets. These plans require a simultaneous two order of magnitude increase in landed mass capability, four order of magnitude increase in landed accuracy, and an entry, descent, and landing operations sequence that may need to be completed in a lower density (higher surface elevation) environment. This is a tall order that will require the space qualification of new EDL approaches and technologies.

In this investigation, the technology challenges associated with improving our landing site access and landed mass capability are reviewed. Approaches being investigated by the robotic Mars exploration program to increase landed mass capability to 0.8 t while improving landed accuracy to 10 km, and landing at a site as high as +2 km MOLA elevation will be described. It will be shown that this class of mission may be the limit for the Viking-era EDL technology that has served us so well for decades. In addition, the entry, descent, and landing sequence for a human exploration system will be reviewed, highlighting the technological and systems advances required for this grand challenge.

II. Mars Entry, Descent, and Landing Challenges

Mars entry, descent, and landing is fraught with systems engineering challenges. These challenges emanate from 1) an atmosphere which is thick enough to create substantial heating, but not sufficiently low terminal descent velocity, 2) a surface environment of complex rocks, craters, dust, and terrain patterns, and 3) the cost of replicating a Mars-relevant environment for space flight qualification of new EDL technologies. In the following discussion, each of these EDL challenges will be addressed and the resulting system impact presented.

A. Atmospheric Density, Opacity, and Landing Site Elevation

Relative to the Earth, the Mars atmosphere is thin, approximately 1/100 in atmospheric density (see Fig. 1). As a result, Mars entry vehicles tend to decelerate at much lower altitudes and, depending upon their mass, may never reach the subsonic terminal descent velocity of Earth aerodynamic vehicles. Figure 2 shows typical

Received 11 May 2006; revision received 7 September 2006; accepted for publication 12 September 2006.

*Associate Professor, Guggenheim School of Aerospace Engineering. AIAA Associate Fellow.
†Chief Engineer, NASA Mars Exploration Program. AIAA Member.

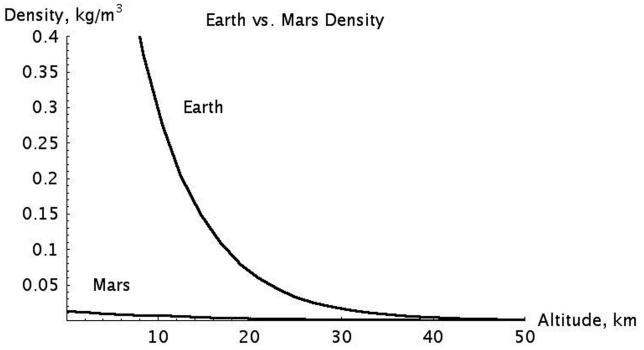

Fig. 1 Earth and Mars atmospheric comparison.

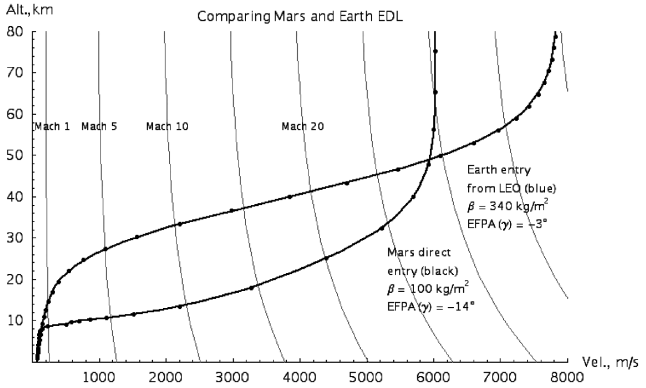

Fig. 2 Altitude-velocity comparison of a typical ballistic EDL at Earth and Mars.

ballistic EDL trajectories for the Earth and Mars, whereas Fig. 3 presents terminal descent velocity at Earth and Mars as a function of entry mass (or ballistic coefficient). Note that on Mars, only entry systems with β below about 50 kg/m^2 have the ability to deliver payloads to subsonic conditions, and only then at altitudes near the surface (below about 10 km). Whereas Earth and Mars have large differences in size and mass (which directly affects entry velocity through gravitational attraction), the largest difference on EDL systems design is the thin Mars atmosphere. As one example, because hypersonic deceleration occurs at much lower altitudes on Mars than on the Earth, the time remaining for subsequent EDL events is often a concern. On Mars, by the time the velocity is low enough to deploy supersonic or subsonic decelerators, the vehicle may be near the ground with insufficient time to prepare for landing.

Atmospheric variability across a Mars year limits our ability to develop a common EDL system. In addition, significant atmospheric

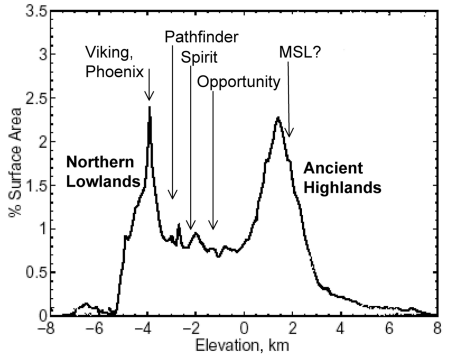

Fig. 4 Mars elevation area distribution.

dust content (a random occurrence) increases the temperature of the lower atmosphere, reducing density, and requiring conservatism in the selection of landing site elevation. The Mars EDL challenge is exacerbated by the bimodal Mars surface elevation, where fully half of the surface of Mars has been out of reach of past landers due to insufficient atmosphere for deceleration. Figure 4 provides the Mars elevation area distribution. The EDL elevation capability of past successful missions and that proposed for the Mars science laboratory is also denoted. To date, all successful Mars landings have been to surface sites with elevation less than −1.4 km MOLA. This technology-imposed requirement has eliminated surface exploration of the ancient terrain in a majority of the southern hemisphere (where the MOLA elevation averages +2 km).

Coupling Mars' low atmospheric density with mission requirements for deceleration has led to entry systems designed to produce a high hypersonic drag coefficient. One such system, the Viking-era 70 deg sphere-cone aeroshell has been used on every U.S. Mars landed mission.

B. Mars Surface Hazards

Landing systems are designed to deliver their payloads within the horizontal and vertical velocity envelops of their touchdown equipment. Despite large visual differences, these landing systems have significant commonality. All of these systems initiate while suspended on a parachute near terminal velocity (between 55 and 90 m/s) and within 1 km of the ground. Despite best efforts, the landing systems flown to date are not tolerant to many potential Mars surface hazards.

Mars has several classes of landing surface hazards. For legged landers, rock hazards are one of the largest challenges. Legged landers built so far have had from 20–30 cm of ground clearance (after leg stroke for landing load attenuation). Rock clearance is also required for the propulsion system. Terminal descent thrusters

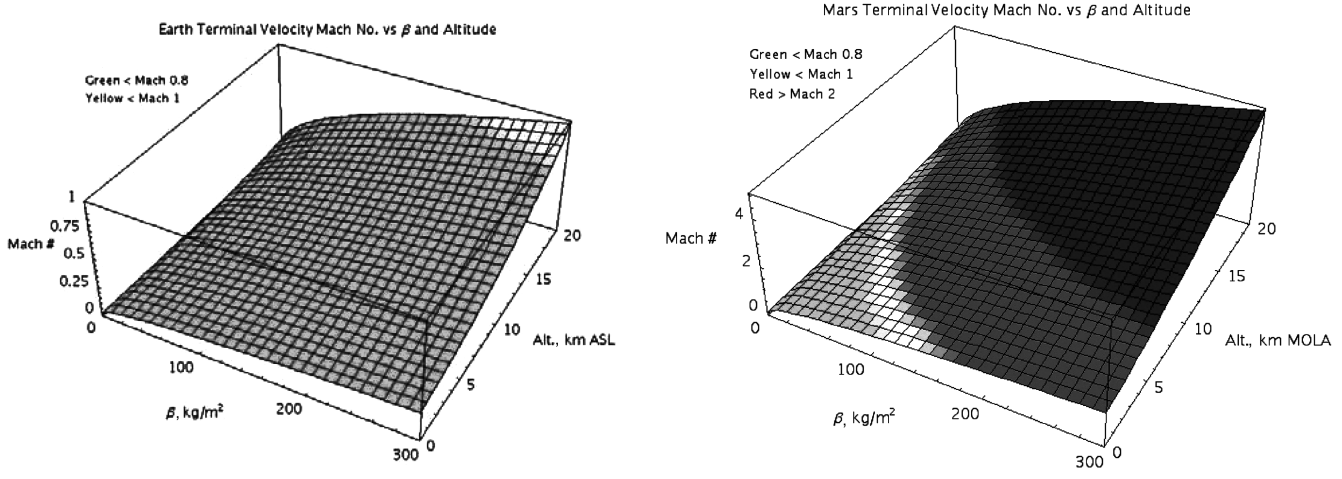

Fig. 3 Terminal descent velocity comparison at Earth and Mars.

cannot spend any more than a few hundreds of milliseconds within a meter or so of the surface without digging trenches, launching small rocks into the landing gear, and producing destabilizing ground-effect backpressure on the bottom of lander. For this reason, legged landers with integrated propulsion systems approach the ground at relatively high-speed (2.4 m/s) with the converse effect of increasing susceptibility to slope-induced tipover hazards.

A surface clearance between 30 and 50 cm is believed to be sufficient for many scientifically interesting landing areas on Mars; however, the ability to directly detect rocks of that size from Mars orbit has not yet been accomplished (the current detection limit is >1 m). Instead, rock size distributions are inferred from the average thermal inertia of the landing area based on thermal response measured from the Viking infrared thermal mapper, Mars global surveyor (MGS) thermal emission spectrometer, and Odyssey thermal emission imaging system instruments. Large fractions of Mars show thermal inertias that are indicative of very rocky surfaces. Golombek et al. [4–6] have determined rock size distributions as a function of thermal inertia. With the arrival of the Mars reconnaissance orbiter, rocks larger than 0.5 m in diameter may become visible from orbit.

Large rocks can also be found in the vicinity of crater rims for unmodified craters larger than about 100 m in diameter. A priori landing site selection practices attempt to limit the number of large craters (with diameters >1 km) within the target landing ellipse; however, craters less than 1 km are difficult to avoid when the target ellipse is on the order of 30×80 km or more. Rocks combined with slopes on the scale of a lander may pose touchdown and tipover hazards as well as potential postlanded solar array deployment interference. Landing site slopes on scales larger than about 3 m are barely visible using stereo and photoclinometry digital elevation maps derived from images from the MGS Mars orbiter camera narrow angle system [7].

Larger scale surface features like hills, mesas, craters, and trenches pose risks not only to the touchdown system, but also to the ground sensors. Radar altimetry and Doppler radar can be "spoofed" by slopes and other surface shapes. Touchdown targeting algorithms such as those used on the Mars exploration rover (MER) and Mars Pathfinder (MPF) can be tricked into releasing the lander early if the vehicle is descending over mesas, trenches, or crater rims. Horizontal velocity errors may be induced when a wide beam from a Doppler radar measures surface-relative velocity over slopes.

When performing Monte Carlo simulations that include all aspects of EDL, including all expected environmental variations, it is common to count the number of times the EDL system encounters conditions that exceed its design capability envelope. For legged systems, Mars surface variability causes the largest source of capability violations. For airbag systems, Mars wind variability (and its resultant affect on touchdown velocity) causes the largest source of capability violations. In both landing systems, environmental conditions result in 2–15% probability of a capability violation (and an associated probability of mission failure). In addition, nonpropulsive landing systems options, airbags, and other mechanical means, are generally limited to landed masses of approximately 0.6 t due to the design and qualification challenges associated with these systems in uncertain, rock-abundant terrain.

C. Space Flight Qualification

Because of the short time span of Mars EDL (on the order of 5–8 min) and the added complexity of switching between units in flight, most key EDL subsystems are nonredundant (single-string). As a result, EDL systems must exhibit high intrinsic reliability in their design environment. Because an EDL end-to-end verification and validation test is not possible on Earth due to differences in the Earth's atmosphere and gravity, substantial simulation is included as part of the flight project's verification and validation process. This end-to-end simulation must be anchored in data obtained from each EDL component's use in past flight projects or Earth-based testing. Unfortunately, the cost associated with reproduction of a Mars-relevant environment for hypersonic and supersonic EDL systems can be quite large. This qualification cost has limited the application of new EDL technologies to those that are derived from past missions with minor modification (argued as having substantial heritage) or qualified in ground-based facilities at a reasonably low cost for the individual project.

III. Past Landed Missions

The first Mars landing attempt (Mars 2) in late 1971 by the Union of Soviet Socialist Republics was a failure; however, the second attempt later that same year (Mars 3) resulted in a partially successful landing and 20 s of transmission from the surface before permanently falling silent.

The five successful U.S. landing attempts began in 1976 with the dual landing of Viking 1 and 2. The Viking mission and the EDL technology developed for Viking became the backbone for all U.S. missions since. More than 20 years later in 1997, the Mars Pathfinder team adapted entry and descent technology from Viking and merged it with the deceptively simple terminal landing architecture employed in 1971 by the Soviets. Most recently, the Mars exploration rover EDL system that landed the Spirit and Opportunity rovers in early 2004 was a significant upgrade of the Mars Pathfinder EDL design. In the coming years, the Phoenix lander (to be launched in 2007), and Mars science laboratory (to be launched in 2009) will apply new variations on these EDL designs. Key entry, descent, and landing parameters for past and upcoming U.S. Mars missions are summarized in Table 1.

The Viking missions of 1976 (see Fig. 5) were largely influenced by the design of lunar landers (lunar Surveyor and Apollo) and were not constrained by today's relatively small budgets. As such, the high-cost to develop new aeroshell, thermal protection, supersonic parachute, Doppler radar, and throttled descent engine systems was accommodated within the overall project cost. Viking's low mass design choice was to use landing legs with small clearances for rocks [8]. Radar altimetry and Doppler radar were used to sense altitude and horizontal velocity. Monopropellant throttled engines were employed to bring the lander to within 2.4 ± 1 m/s vertically and <1 m/s horizontally. These choices were made based on the science team evaluation that the selected Mars landing sites were relatively flat and rock-free. Once on Mars, however, the Viking designers were surprised to see large rocks so close to the lander. Fig. 6 shows Big Joe, approximately 2 m long and 1 m high, located approximately 8 m from the Viking 1 landing site. The Viking landers were designed with a 20 cm rock clearance.

Mars Pathfinder in 1997 was influenced by the need for extreme cost savings (relative to Viking) and the design of past lunar and Mars landers as well as U.S. Army payload delivery systems [9]. Mars Pathfinder's approach to reduce cost was to use the Viking entry and parachute systems (with passive attitude control) and low cost solid rocket engines that would protect the lander from a much larger range of touchdown velocities than legged landers could handle. This approach would also eliminate the need for horizontal velocity estimation with Doppler radar. The consequence of these design decisions was the need for a heavy and difficult-to-test 4π steradian airbag system that could handle initial vertical velocities as high as 16 m/s and horizontal velocities as high as 22 m/s with the potential for tens of bounces on rocks as high as 0.5 m and 30 deg slopes (see Fig. 7).

The MER missions, arising from the programmatic turbulence after the loss of two Mars missions in late 1999, were most largely driven by schedule. These missions (proposed in April 2000) were intended to use the MPF EDL design so that the schedule to the summer 2003 launch date could be achieved. There was no initial plan to modify the MPF EDL system. However, as further information was gained (50% higher suspended mass than MPF and higher than originally anticipated winds), it was discovered that the MPF terminal descent heritage was not sufficient to deliver the MPF airbags to an acceptable velocity envelope [10,11]. New horizontal control systems (inertial measurements and small solid rocket motors in the backshell) and new horizontal velocity estimation using descent imagery were added to ensure sufficient EDL system

Table 1 Past successful and currently proposed U.S. Mars EDL summary

Landing year:	1976	1976	1997	2004	2004	2008	2010
Mission:	Viking 1	Viking 2	MPF	MER-A (Spirit)	MER-B (Opportunity)	Phoenix (planned)	MSL (planned)
Entry from	orbit	orbit	direct	direct	direct	direct	direct
Inertial entry velocity, km/s	4.7	4.7	7.26	5.4	5.5	5.59	<6.0
Orbital direction	posigrade	posigrade	retrograde	posigrade	posigrade	posigrade	either
Inertial entry flight-path angle, deg	−17	−17	−14.06	−11.49	−11.47	−13	−15.2
Ballistic coefficient, kg/m^2	64	64	63	94	94	65	115
Entry mass, kg	992	992	584	827	832	600	2920
Entry attitude control	3-axis RCS	3-axis RCS	2 RPM passive	2 RPM passive	2 RPM passive	3-axis RCS	3-axis RCS
Trim angle of attack at entry	−11 deg	−11 deg	0 deg	0 deg	0 deg	0 deg	−15 deg
Entry lift control	center-of-mass offset	center-of-mass offset	no offset	no offset	no offset	no offset	center-of-mass offset
Entry guidance	unguided	unguided	unguided	unguided	unguided	unguided	Apollo guidance
Lift-to-drag ratio	0.18	0.18	0	0	0	0	0.24
Aeroshell (heat shield) diameter, m	3.5	3.5	2.65	2.65	2.65	2.65	4.5
Heat shield geometry	70 deg cone	70 deg cone	70 deg cone	70 deg cone	70 deg cone	70 deg cone	70 deg cone
Heat shield TPS	SLA-561	SLA-561	SLA-561	SLA-561	SLA-561	SLA-561	SLA-561
Heat shield TPS thickness, in.	0.54	0.54	0.75	0.62	0.62	0.55	0.9
Total integrated heating, J/m^2	1100	1100	3865	3687	3687	2428	<6200
Peak heating rate, W/cm^2	26	26	100	44	44	47	<210
DGB parachute diameter, m	16	16	12.5	14	14	11.7	19.7
Chute drag coefficient (approx.)	0.67	0.67	0.4	0.4	0.48	0.62	0.67
Parachute deploy Mach no.	1.1	1.1	1.57	1.77	1.77	1.2	2.2
Chute deploy dyn. pressure, Pa	350	350	585	725	750	430	750
Parachute deploy altitude, km	5.79	5.79	9.4	7.4	7.4	9.8	6.5
Descent attitude control	RCS roll rate	RCS rate	none	none	none	RCS roll rate	RCS roll rate
Altitude sensing	radar	radar	radar	radar	radar	radar	radar
Altitude sensing range, km	137	137	1.6	2.4	2.4	1.6	6
Horizontal velocity sensing	Doppler radar	Doppler radar	none	descent imaging/IMU	descent imaging/IMU	Doppler radar	Doppler radar
Terminal descent decelerator	monoprop N2H4	monoprop N2H4	solid rockets	solid rockets	solid rockets	monoprop N2H4	monoprop N2H4
Terminal descent velocity control	throttled	throttled	sep. cutoff	sep. cutoff	sep. cutoff	duty-cycle pulse	throttled
Horizontal velocity control	throttled pitch	throttled pitch	passive	lateral SRMs	lateral SRMs	throttled pitch	throttled pitch
Touchdown vertical velocity, m/s	2.4	2.4	12.5	8	5.5	2.4	0.75
Touchdown horizontal velocity, m/s	<1	<1	<20 (design)	11.5	9	<1	<0.5
Touchdown attenuator	3 crushable legs	4 crushable legs	4π airbag	4π airbag	4π airbag	3 crushable legs	6 wheels
Touchdown rock height capab., cm	20	20	50	50	50	30	100
Touchdown slope capab., deg	15	15	>30	>30	>30	15	>15
Touchdown sense	leg crush motion	leg crush motion	rollstop	time-out	time-out	leg crush motion	off load
Touchdown sensor	——	——	accelerometer	clock	clock	hall effect	throttle down
Touchdown mass, kg	590	590	360	539	539	382	1590
Useful landed mass, kg	244	244	92	173	173	167	800
3-sigma landed ellipse major axis, km	280	280	200	80	80	100	20
3-sigma landed ellipse minor axis, km	100	100	100	12	12	21	20
Landing site elevation, km MOLA	−3.5	−3.5	−2.5	−1.9	−1.4	−4.0	2.0

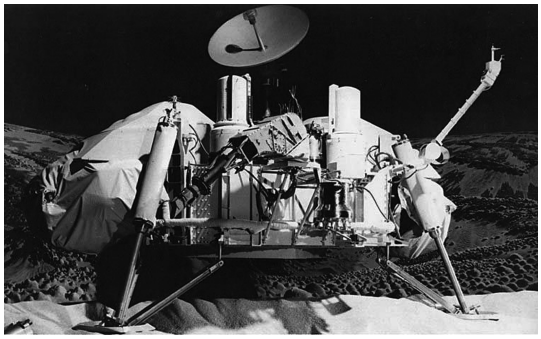

Fig. 5 Viking lander.

Fig. 6 Big Joe at the Viking 1 landing site.

reliability. In addition, the MPF airbags were redesigned and toughened to handle the higher mass of the payload, and to survive higher impact velocities, up to 26 m/s.

The Phoenix mission, planned for launch in 2007 (see Fig. 8), is based on the design of the Mars Polar Lander mission that was lost during its landing attempt in 1999 [12]. This mission was also driven by the need for cost savings. Relatively expensive horizontal Doppler radar velocity measurement was avoided by using canted multibeam radar. Expensive throttled engines were avoided by using off-pulsed engines at high-duty cycles. Although not as tolerant of rocks and slopes as the MPF/MER touchdown system, the ability to find areas on Mars less rocky and with lower slope will allow Phoenix to land safely. Recent full-scale testing of the duty-cycle modulated propulsion system has demonstrated that the pulsed-mode engine firing is robust.

The Mars science laboratory (MSL) landing system, planned for launch in 2009, forges new ground in touchdown system design [13]. One of the major design constraints for propulsive descent landers (where the descent engines must fire very close to the ground) is to use a low surface pressure plume or to spend a minimum amount of time in the vicinity of the surface. These constraints are meant to

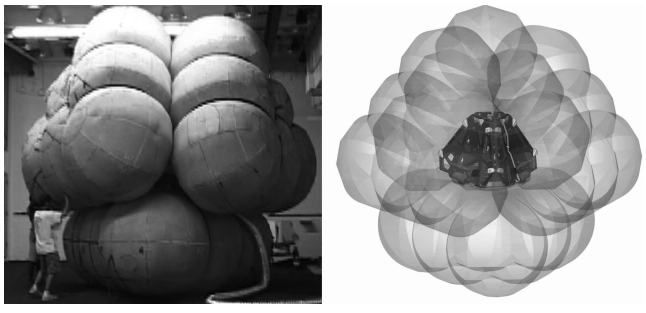

Fig. 7 Mars Pathfinder and MER airbags.

Fig. 8 Phoenix lander.

avoid creating hazardous pits in the surface and throwing rocks and dirt on top of the delivered payloads. This minimum time descent is accomplished by descending as fast as the landing gear will allow, exacerbating the need for ground clearance of high rocks under the vehicle and slope tolerance. Positioning the terminal propulsion system and its propellant tanks under a rover also presents egress challenges to the landed system. The realization that the MPF/MER terminal descent propulsion system (the solid rocket motors) in the backshell suspended above the lander could be "upgraded" to throttled monopropellant engines resolved this conflict. By virtue of their relatively large distance to the surface, descent engines suspended above the payload could deliver the system to the surface with much lower velocity without a significant increase in propellant (see Fig. 9). This descent system (dubbed the skycrane after its namesake helicopter) eliminates the need for a heavy landing system while at the same time providing increased tolerance of the lander to slopes and rocks [13]. In fact, MSL is planning to land the rover directly onto its wheels without modifying the design of the rover mobility system. The MSL EDL system has the potential to someday allow Mars landed payloads to be designed independent of EDL, much as launch vehicles are today.

IV. Current Entry, Descent, and Landing Technology Limits

Many of the EDL systems discussed in the preceding section were originally developed as part of the focused technology development effort that preceded the Viking landings. In addition to the first planetary landings, the Viking program developed the 70 deg sphere-cone aeroshell, the SLA-561V forebody thermal protection material, and the supersonic disk-gap-band (DGB) parachute. With minor modification, these three EDL components have formed the backbone of all Mars EDL architectures since. As the Mars robotic exploration program strives to deliver more mass to higher elevation sites with improved landed accuracy, one might ask, how far can these and other Viking-era EDL technologies take us?

A. Seventy Degree Sphere-Cone with SLA-561V Forebody Thermal Protection System

A scaled variant of the Viking 70 deg sphere-cone aeroshell (see Fig. 10) has been employed on every Mars landing mission due to its

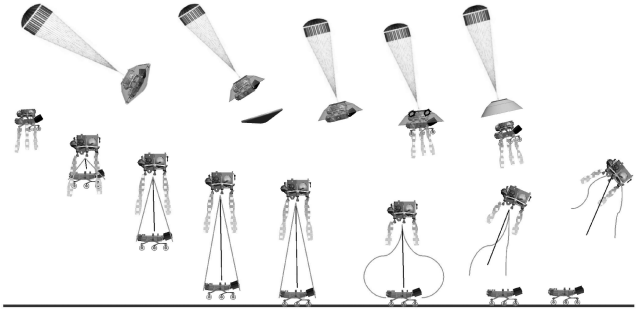

Fig. 9 MSL skycrane descent sequence.

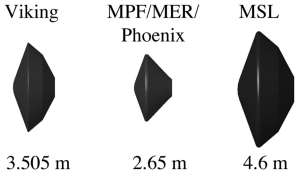

Fig. 10 Viking-heritage 70-deg sphere-cone aeroshells.

relatively high hypersonic drag coefficient (zero angle-of-attack hypersonic C_D of approximately 1.68) and the existence of a broad set of aerodynamic performance data on this shape. This aeroshell configuration has been flown successfully along different entry trajectories and at angles-of-attack between zero and 11 deg. A different aeroshell forebody shape will not have a significant impact on hypersonic drag coefficient and therefore cannot be relied upon as a means to improve EDL performance.

An entry system's deceleration and heating profile is governed by its hypersonic ballistic coefficient, which is defined by its mass, drag coefficient, and reference areas as

$$\beta = \frac{m}{C_D A}$$

A low ballistic coefficient vehicle will achieve lower peak heat rate and peak deceleration values by decelerating at a higher altitude in the Mars atmosphere. This system will be characterized by more timeline margin for the subsequent descent and landing events. To reduce ballistic coefficient, systems engineers tend toward the largest aeroshell diameters possible, where this diameter is generally limited by physical accommodation within launch vehicle and/or integration and test facilities. Cost requirements of recent robotic missions (MPF, MER, and Phoenix) have led to reliance on Delta 2 class launch vehicles whose launch shrouds have limited the aeroshell maximum diameter to 2.65 m. However, for the cost increment of the Atlas 5 class launch system, aeroshell diameters as large as 4.6 m may be considered.

To date, β has ranged from 63 to 94 $\mathrm{kg/m^2}$ (see Table 1). Because ballistic coefficient is a significant driver on parachute deployment altitude and the subsequent EDL events timeline, as landed mass is increased, the aeroshell diameter must also increase. It is for this reason that the Mars science laboratory project has adopted a 4.5 m diam 70 deg sphere-cone aeroshell, where the 4.5 m diam constraint is imposed by existing integration and test facilities [2].

For landed masses above the 0.8 t proposed for MSL, launch shrouds larger than any currently in existence or large increases in ballistic coefficient (up to density limits dictated by aeroshell packaging) will be required. Using the extraordinarily high, packaged density of the MER aeroshell as an upper-limit and noting that to first-order, β increases linearly with diameter, the maximum β for a 4.6 diam 70 deg sphere-cone is approximately 153 $\mathrm{kg/m^2}$. This is the largest β one can imagine for robotic Mars systems over the next several decades.

Although such a system may be designed to successfully transit the hypersonic flight regime, Fig. 11 shows the impact of ballistic coefficient on parachute deploy altitude. Assuming a fixed time requirement for the subsonic descent to the surface allows for examination of the relationship between β and landing site surface elevation. For ballistic entry, the parachute deploy altitude of the $\beta = 153$ $\mathrm{kg/m^2}$ case is 7.3 km lower than for the $\beta = 63$ $\mathrm{kg/m^2}$ case. The advantage of aerodynamic lift is also evident in Fig. 11, resulting in a potential increase of 4–5 km at parachute deployment. Figure 11 trajectories assume an entry velocity of 6 km/s, nominal

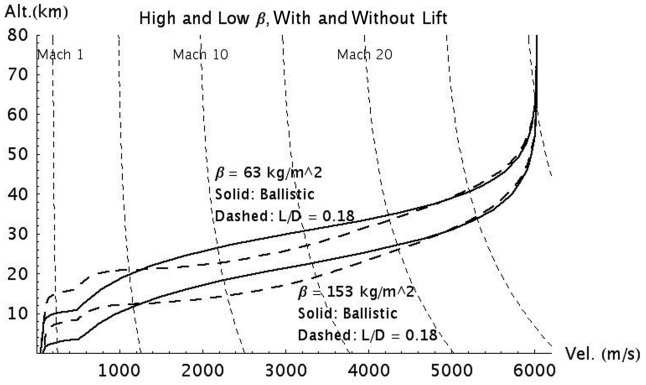

Fig. 11 Mars EDL nominal trajectories deploying a 19.7-m-diam parachute at Mach 2.1.

low-τ (0.3) midlatitude atmosphere, use of a 19.7-m-diam parachute deployed at Mach 2.1 with C_D of 0.65, and a 15 s timeline from Mach 0.8 to 1 km (start of propulsive descent). In addition, 75% of the $L/D = 0.24$ (vertical $L/D = 0.18$) is used to manage the altitude channel and each trajectory has an entry flight-path angle selected to maximize parachute deploy altitude.

Once off-nominal effects are included, an approximate landing site elevation limit may be derived as a function of β and vertical L/D. Applying 3-σ dispersed atmospheric, aerodynamic, and parachute targeting uncertainties, the landed site elevation capability (including dispersions) is shown in Table 2 as a function of β. To deliver additional mass over that listed in Table 2 to a given surface elevation, one must either reduce the hypersonic ballistic coefficient of the entry system, reduce the altitude/timeline requirements of the subsequent EDL events, or introduce new decelerator technology to reduce the supersonic descent ballistic coefficient.

High β vehicles and larger diameter aeroshells will also suffer from additional aerothermodynamic heating and uncertainty in the prediction of that heating due to radiative effects and transition to turbulence [14,15]. For such systems, the peak heat rate is likely to be located along the conical flank of the forebody, as opposed to the nose region of the vehicle; as a result, shear effects may be significant. This is a more difficult aerothermodynamic environment and aeroshell location to accurately replicate in ground-based testing, introducing additional uncertainty in the TPS qualification approach. As the heat rate increases above several hundred $\mathrm{W/cm^2}$, the heritage of the SLA-561V material must be reaffirmed or a new material qualified for flight. While not directly affecting the aeroshell shape, such a qualification program will likely be expensive and require upfront planning of the development schedule.

B. Supersonic Disk-Gap-Band Parachute

As shown in Fig. 3, the terminal velocity of a Mars entry system is generally larger than a few hundred m/s. While this is much slower than the several km/s entry velocity, it is too large an impact velocity for a lander. As a result, all previous and currently planned EDL architectures deploy a supersonic parachute to decrease the descent β and slow the vehicle to subsonic speeds before too much altitude is lost. Besides the added drag, the parachute also provides sufficient vehicle stability through the transonic regime and the marked decrease in descent β allows for positive separation of the aeroshell forebody (heat shield), a critical step in reconfiguration of the system for landing.

Table 2 Approximate landed mass constraint as a function of elevation (including dispersions)

Surface elevation, MOLA km	Maximum β, $\mathrm{kg/m^2}$	Landed mass for 2.65-m-diam aeroshell	Landed mass for 4.5-m-diam aeroshell
−2.0	160	350	1000
0.0	135	300	850
+2.0	115	250	750

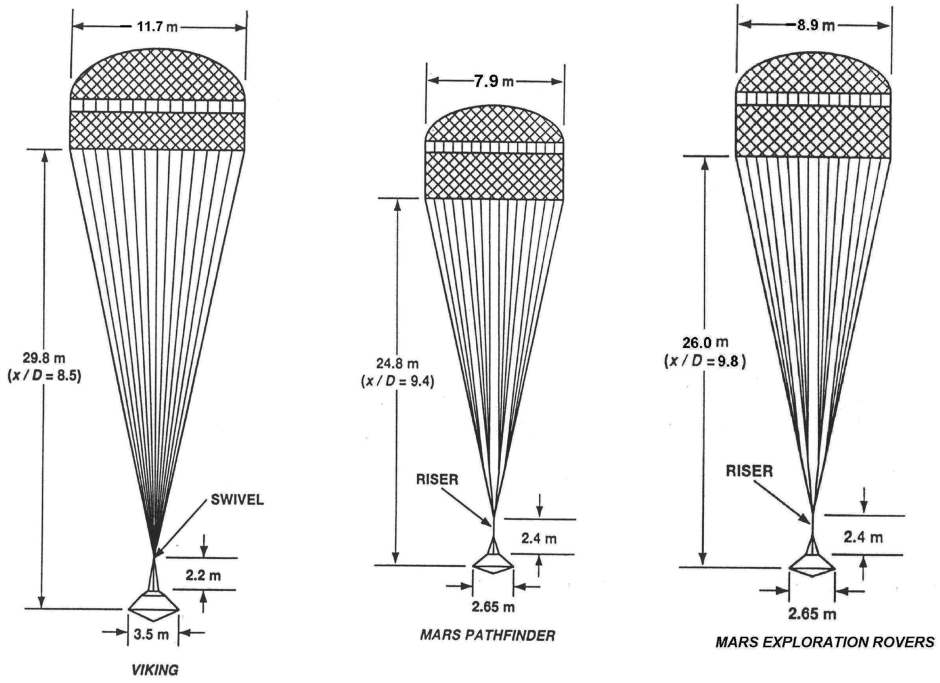

Fig. 12 Viking-derived parachute systems.

Analogous to the 70-deg sphere-cone, all of the Mars landing systems in Table 1 use parachute systems derived directly from the Viking parachute development program. In 1972, high-altitude, high-speed qualification tests of the Viking parachute in Earth's atmosphere were successfully conducted in Mars-relevant conditions [16]. These tests showed the Viking parachute design would robustly deploy, inflate, and decelerate the payload in the expected flight conditions. Because of the expense of these tests, their like has not been attempted since. Instead, all subsequent Mars EDL systems including those planned in the foreseeable future rely on inflation qualification by similarity to the Viking design and focus on parachute strength qualification through lower-cost subsonic and static testing [17–19].

The Viking project selected a disk-gap-band parachute, shown in Fig. 12, whose acronym directly describes the construction of the parachute from a disk that forms the canopy, a small gap, and a cylindrical band. The Viking parachute system was qualified to deploy between Mach 1.4 and 2.1, and a dynamic pressure between 250 and 700 Pa, a considerable margin relative to the Viking flight values of Mach 1.1 and a dynamic pressure of 350 Pa. This system had a 16 m diam.

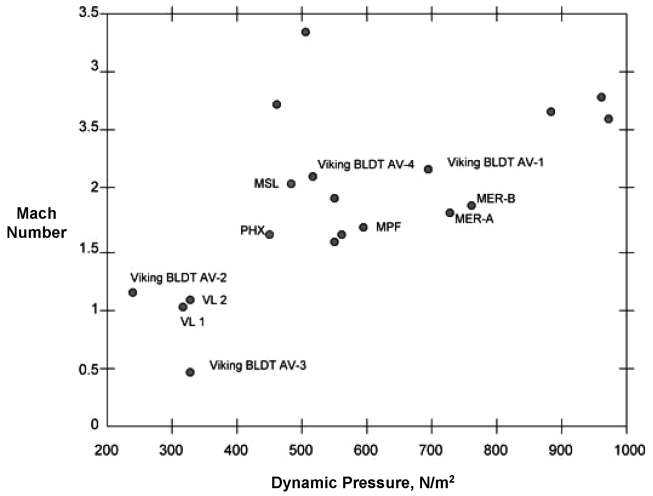

Fig. 13 Mach and dynamic-pressure history for successful inflation disk-gap-band parachutes in Mars-relevant conditions [18].

Post-Viking applications of the DGB design varied the size and relative proportions of the parachute to trade stability vs drag, but were careful not to invalidate the Viking inflation qualification. The Viking, Mars Pathfinder, and Mars exploration rover parachutes all performed their functions admirably at deployment Mach numbers as high as 1.8 and a dynamic pressure as high as 780 Pa (see Fig. 13). Both MER and MPF used smaller diameter supersonic parachutes as they delivered less mass to the Mars surface.

The Mars science laboratory has baselined a larger diameter supersonic parachute than the one flown on Viking. This increase in parachute size is required due to the large descent mass and also to maintain scaling with the aeroshell diameter used in the Viking qualification program. Fortunately, the Viking qualification program included a parachute test (19.7 m diam) of the size planned for MSL, and so this Viking test result applies directly to the planned MSL parachute qualification.

The MSL payload mass of 0.8 t may be the largest payload capable of delivery to a +2 km MOLA elevation with Viking-era parachute technology. As we look to larger, greater than 1 t delivered systems, we will break out of the Viking qualification regime with respect to parachute size due to the need for larger aeroshell diameters and rapid deceleration to preserve timeline. As depicted in Fig. 11, higher β entry systems reach the parachute deployment Mach limit at significantly lower altitudes with an associated loss of timeline for the subsequent EDL events. And so, in addition to larger size, a higher deployment Mach number may also be required (perhaps as high as parachute material temperature limits will allow, approximately Mach 2.7). These greater requirements will mandate a new high-altitude supersonic qualification program to enable those missions. Such a qualification program will be expensive and require upfront planning of the development schedule.

Once subsonic conditions are achieved, a larger parachute that is less expensive to qualify can be deployed to reduce the velocity further and hence the requirements on the terminal descent system, as well as potentially provide added time for the lander reconfiguration and sensing events. For large mass landed systems, such staged parachute systems may provide compelling system benefits that outweigh their inherent complexity and risk [20–22].

C. Landed Accuracy

To date, no Mars entry system has used a real-time hypersonic guidance algorithm to autonomously adjust its flight within the Mars

atmosphere. MPF and MER flew ballistic entries and had no means of exerting aerodynamic control over the atmospheric flight path. As such, the design landing footprints were relatively large (200 km in 3-σ downrange for MPF and 80 km for MER). Whereas Viking flew a lifting trajectory, it did not use this lift to adjust the vehicle's flight path to real-time uncertainties in the entry navigation or atmospheric conditions, and instead flew a lift-up entry to improve the EDL timeline and mitigate concerns in regard to achieving the appropriate deceleration in the thin Mars atmosphere.

Using the MER entries as a baseline, the addition of improved approach navigation (e.g., delta differential one-way range, dual spacecraft tracking and optical navigation) can reduce the 3-σ landed footprint of a ballistic entry to 60–80 km in major axis, where the dominant error source becomes uncertainty in the Mars atmospheric density [23]. To improve landed accuracy further, atmospheric and aerodynamic uncertainties must be mitigated during the atmospheric flight [24,25].

The Mars science laboratory will take the first major step toward performing precision landing at Mars [3]. Using hypersonic aeromaneuvering technology and improved approach navigation techniques, this spacecraft should set down within 10 km (3-σ) of the specified science target. This is essentially an order of magnitude improvement over the Mars Pathfinder, MER, and Phoenix ballistic entries. Such an advance in delivery uncertainty is possible as a result of improved interplanetary navigation techniques and the qualification for flight of a lifting aeroshell configuration directed by an autonomous atmospheric guidance algorithm that controls the aeroshell lift vector during the high dynamic-pressure portion of atmospheric flight [24]. In this manner, based on in-flight measurements of deceleration, the guidance algorithm can autonomously maneuver the vehicle toward a more or less dense atmosphere region, thereby accommodating off-nominal entry-state or atmospheric-flight conditions. Whereas numerous guidance algorithms have been developed for use during hypersonic flight, this will be the first flight of a lifting entry vehicle directed by an autonomous atmospheric guidance algorithm at Mars. This is a major advancement of planetary exploration EDL technology.

During the approach to Mars, position and velocity estimation is performed by the mission navigation team based on radiometric tracking measurements obtained through the deep space network. These ground-based estimates are used to initialize the spacecraft inertial measurement unit (IMU) a few hours before entry. During the Mars hypersonic flight phase, position and velocity knowledge is maintained by the IMU. With use of a low L/D aeroshell, an autonomous atmospheric guidance algorithm, and an accurate IMU, relatively large approach navigation delivery errors (entry flight-path angle errors on the order of 0.3–0.5 deg) can be mitigated in the presence of large dispersions in atmospheric density and vehicle aerodynamics [24,25]. Furthermore, with use of a high-accuracy IMU, the vehicle's position knowledge error at parachute deployment can be effectively reduced to the navigation knowledge error at IMU initialization as a result of the short entry flight duration. Given that the landed system is likely to drift (uncontrolled) for several kilometers while descending under the parachute, this knowledge initialization error can be on order of a few kilometers (with respect to inertial space) without being the largest contributor to the landed inertial position accuracy.

V. Advancing Beyond Viking EDL Technology: Implications for Future Robotic Missions

As discussed in the preceding section, landing a Mars payload of approximately 0.8 t at a landing site of +2 km MOLA elevation is stretching the limits of our Viking-era EDL technology. However, there are several EDL technologies that show promise to deliver additional mass to the Mars surface. Some of these technologies may prove to be required for advanced robotic science missions like the Mars sample return (MSR) and astrobiology field laboratory (AFL).

To view this challenge, the physical constraints of EDL must be illuminated. As discussed in Sec. IV, one such constraint is the present supersonic parachute deployment dynamic pressure and

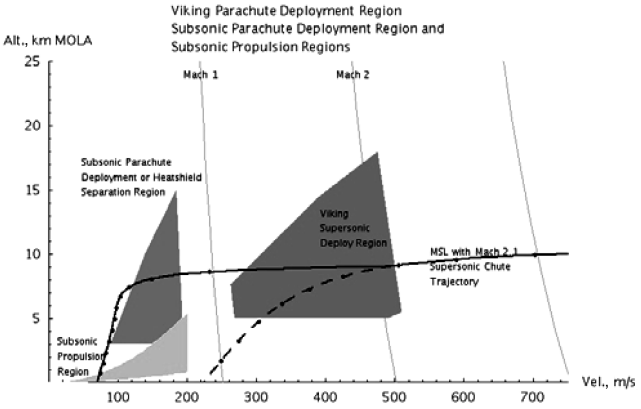

Fig. 14 Supersonic parachute deployment region, subsonic deployment regions.

Mach qualification region. This constraint region is shown in Fig. 14. The trajectory of a Viking-heritage entry, descent, and landing system must pass into this region to deploy a supersonic parachute. In Fig. 14, this region is bounded by Mach 2.1 and Mach 1.1 on the upper right, and left, a dynamic pressure limit of 250 Pa on the top, 1200 Pa on the lower right, and finally 5 km MOLA altitude on the bottom. The lower altitude limit is a surrogate for the descent timeline from parachute deployment to the ground. Unless the mission happens to be targeting a Mars region with relatively low landing site elevation, this 5 km altitude limit is slightly aggressive.

Figure 14 also shows a lifting entry trajectory for a vehicle with vertical L/D of 0.18 and a β of 100 kg/m^2. This trajectory is similar to that proposed for the Mars science laboratory project. The trajectory travels right-to-left into the supersonic parachute deployment region before inflating a 19.7-m-diam parachute at Mach 2.1. Note that without a parachute, this entry system would impact the surface at approximately Mach 1 (dashed line). Figure 14 also depicts two other regions. The subsonic region is bounded by Mach 0.8 on the right, a dynamic pressure of 50 Pa on the left side, and 3 km MOLA altitude on the bottom. Subsonic parachutes must be inflated at or below Mach 0.8 due to drag loss near Mach 1. This is the region where aeroshell separations and deployments may occur. The subsonic propulsion region is bounded by Mach 0.8, a thrust-to-Mars-weight upper limit of eight and a lower limit of two. These constraints suggest several alternatives for the delivery of large mass payloads, which are discussed in the following sections:

1) Reduce the hypersonic ballistic coefficient below 50 kg/m^2 through a large increase in reference area.

2) Extend the supersonic parachute deployment region to the right, to even higher Mach numbers.

3) Increase vertical lift without a reduction in drag.

4) Develop a new supersonic decelerator that can "capture" the entry vehicle state higher and faster.

A. Reduction in Hypersonic Entry Ballistic Coefficient

As mass grows, β will increase and the entry trajectory will eventually fall short of the supersonic parachute deployment region. Figure 15 shows the effect of increasing β from 25 to 200 kg/m^2 while fixing lift and entry flight-path angle. When β gets above approximately 150 kg/m^2, the trajectories fall below the supersonic parachute deployment region and a Viking parachute cannot be used for aerodynamic deceleration. This is termed the "supersonic transition gap" and implies large aeroshell diameter requirements for a large payload mass. Without significant modification of the hypersonic entry trajectory, high β entry vehicles cannot land on Mars.

One alternative is to decrease β and enter with a very large hypersonic decelerator. As shown in Fig. 15, blunt body entry vehicles with β on the order of 25 kg/m^2 eliminate the need for a separate supersonic decelerator. These systems would simply require a drogue for stabilization in the transonic regime and a large subsonic parachute or propulsive decelerator. For a 1 t lander, the aeroshell

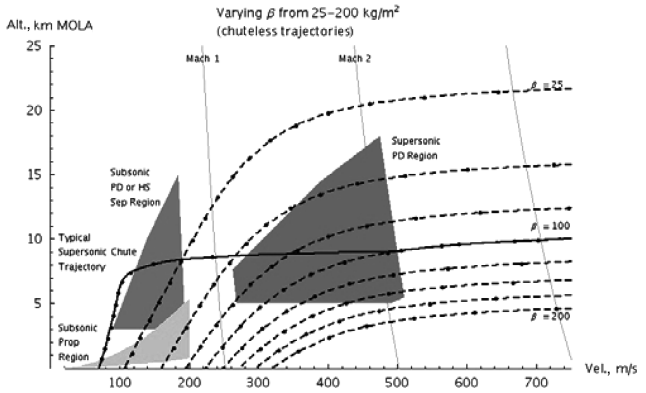

Fig. 15 EDL feasibility as β is increased from 25–200 kg/m^2.

would have to be about 11.5 m in diameter. Without on-orbit construction, an inflatable or deployable entry aeroshell is a logical option. Full-scale testing of these systems on Earth under Mars-like conditions will be required (at high-altitude and at hypersonic speeds). Although much work remains to qualify inflatable and deployable hypersonic entry aeroshells for Mars, this technology appears promising for larger mass robotic systems [26]. As an intermediate step, one could use an inflatable system below Mach 5 where the aeroheating environment is much lower than at hypersonic speeds [27].

B. Extension in the Parachute Deployment Region

Extension of the disk-gap-band inflation Mach region to Mach 2.7 or Mach 3 may be possible using stronger and more heat-resistant fabrics (see Fig. 16). The parachute structure would also have to be designed to higher inflation dynamic pressures (well above 1200 Pa). Low-density, high-Mach Earth tests have shown an indication of dynamic instability above Mach 2.5 that may require significant new high-altitude and high dynamic-pressure flight tests [17]. In addition, if larger diameter parachutes were qualified, the descent rate would be reduced allowing the lower bound of the parachute deployment region (which is timeline constrained) to be reduced. This is another approach to expanding the supersonic parachute deployment envelope. The Mars program has studied what it would take to develop and qualify a 30 m diam Mach 2.7 disk-gap-band parachute. This parachute is 50% larger in diameter and would provide 2.3 times the drag than the largest Viking chute ever tested. As it was in the 1960s, this test program would be technically challenging and costly [17]. Although this development would likely enable the robotic MSR and AFL missions, other solutions must be found for missions that approach human-scale exploration >20 t.

C. Supersonic Propulsion

An additional supersonic decelerator possibility is simply to use propulsion. Whereas this appears straightforward, there is little experience firing larger thrusters directly into a high dynamic-pressure supersonic flow. Flow stability, flow-control interaction, and thermal protection are some of the design issues that surround use of this technology. This technology development option may provide a strong link between advanced robotic landers and those required for eventual human exploration.

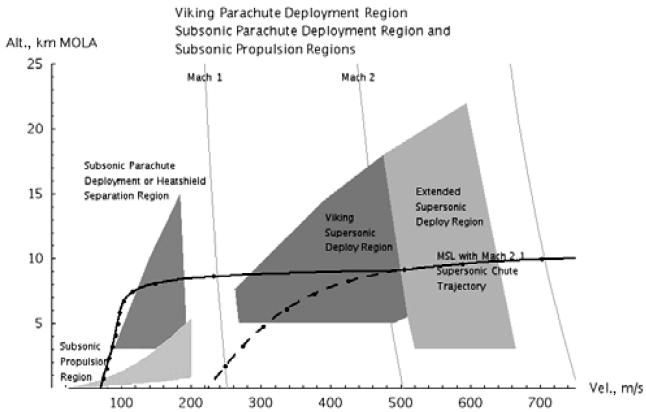

Fig. 16 Potential extension of the Viking supersonic parachute deployment region.

D. Increased Vertical Lift of the Entry Body

With additional vertical lift, a large mass entry system may be able to regain sufficient altitude to enter the Viking supersonic parachute deployment region. However, care must be taken to avoid designing in additional lift at the expense of drag area, and hence a corresponding β penalty. Figure 17 shows the affect that increasing the vertical L/D from 0.2 to 0.5 has on the trajectory. The addition of lift (without significant loss of drag) may allow entry vehicles with β as high as 200 kg/m^2 and vertical L/D greater than 0.2 to enter the supersonic parachute deployment region. Likewise, entry vehicles with β as high as 250 kg/m^2 with vertical L/D greater than 0.25, and 300 kg/m^2 with vertical L/D greater than 0.3 may be able to enter this region.

Parachute capability after supersonic inflation poses other constraints that may limit vehicle mass (and hence β). In particular,

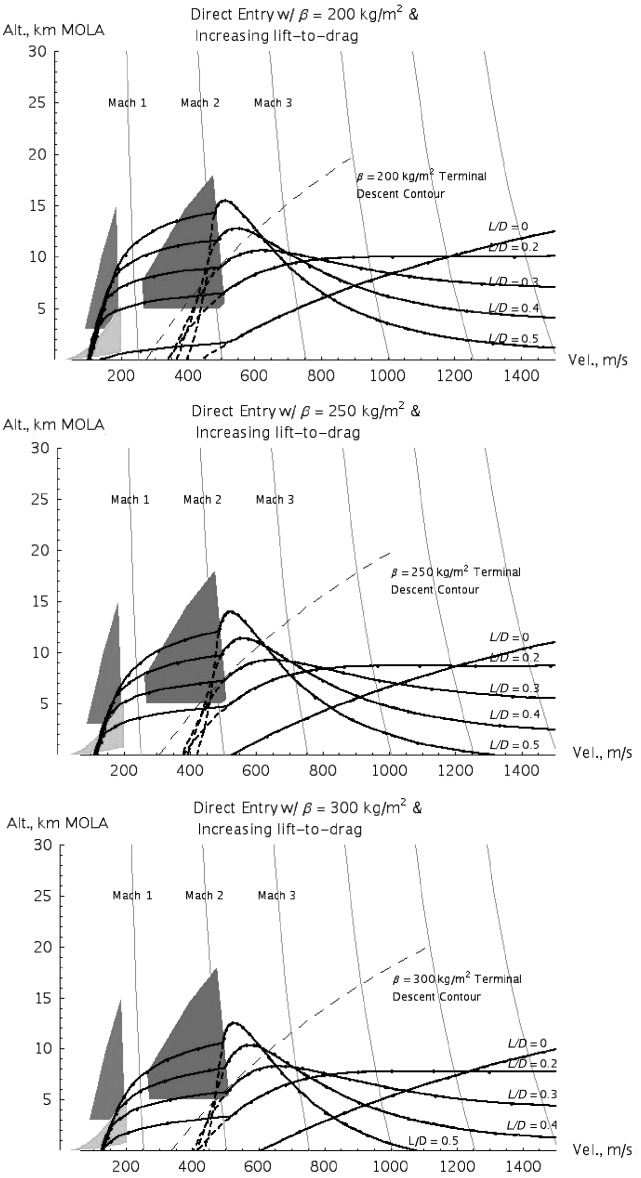

Fig. 17 Increasing vertical lift for entry system with β = 200, 250, and 300 kg/m^2.

to provide sufficient time to configure the vehicle for landing before reaching the ground, the descent β must be below 35 kg/m^2. This implies large parachute diameter requirements for high entry masses (high β cases).

E. Next Steps in Mars Robotic Entry, Descent, and Landing

Robotic Mars missions in the 2010 decade will likely require larger landed mass than has been delivered to date. If these systems require delivery of 2 t on the Mars surface (or 1 t to high surface elevations), at least one of the preceding technology options will need to be exercised. It is likely that the parachute Mach and/or diameter options will be exercised first as these require extension of existing qualified technology; however, if studies and efforts for eventual human Mars EDL are prioritized, future robotic systems may be required to introduce greater technology leaps in preparation for an eventual landing of astronauts on Mars. In addition, improvement in landed precision beyond the 10 km (3-σ) MSL delivery footprint is possible for future robotic systems that obtain surface imagery during the parachute descent and perform autonomous comparison with onboard maps to determine terrain-relative position. Through the addition of a capable descent imager, rapid image processing algorithms, powered descent guidance, and maneuvering propellant, the effect of wind drift and other error sources may be mitigated, yielding landing accuracies of order 100 m (3-σ) [25].

VI. Human Exploration Entry, Descent, and Landing Reference Architecture and Technology Challenges

Target capabilities for robotic spacecraft in the 2010 decade include landing 1–2 t payloads with a precision of less than 10 km, at high-altitude landing sites (+2 km MOLA). These capabilities are quite modest in comparison to the requirements of landing human crews on Mars, which may imply landing 40–80 t payloads with a precision of tens of meters, possibly at high-altitude. New EDL challenges imposed by the large mass requirements of human Mars exploration include 1) the need for aerocapture before EDL and associated thermal protection strategies, 2) large aeroshell diameter requirements, 3) severe mass fraction restrictions, 4) rapid transition from the hypersonic entry mode to a descent and landing configuration, 5) the need for supersonic propulsion initiation, 6) landing accuracy and surface-rendezvous imposed no-fly zones, and 7) increased system reliability [28]. In this section, an entry, descent, and landing architecture for human Mars exploration is presented, highlighting the technology challenges and advances required.

A. Aerocapture

Aerocapture, a single-pass atmospheric maneuver designed to transfer directly from a heliocentric arrival trajectory into the proper Mars staging orbit, has been proposed for several robotic missions but never attempted (see Fig. 18). For robotic missions to Mars, it has been shown that the benefits of aerocapture are relatively small compared with an aerobraking mission [29]. However, for human exploration, aerocapture followed by a subsequent entry and descent to the surface from orbit has several advantages, including significant mass reduction relative to propulsive orbit insertion, mission design flexibility, the ability to accommodate uncertain atmospheric conditions (e.g., dust storms), reduced peak entry deceleration for the human crew relative to direct EDL, and significant time savings relative to aerobraking. The operational flexibility gained from dwelling in orbit before landing mitigates the risk of atmospheric uncertainty. In addition, aerocapture is applicable to components of the human exploration architecture that never land on the surface, but instead dwell in Mars orbit for later rendezvous and Earth return. Although aerocapture is an untried technology, it will likely be required for human missions to bring mass requirements into a feasible range.

A parametric study of aerocapture trajectories was performed to explore the design space for vehicles of a scale suitable for human exploration [28]. Aerocapture trajectories may be constrained by several limits:

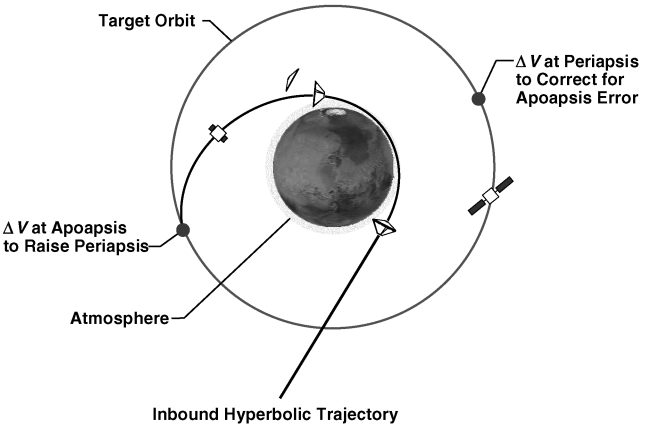

Fig. 18 Mars aerocapture maneuver.

1) The trajectory with the most shallow flight-path angle that meets the exit energy constraint (lift-down) which results in the lowest peak heating rate and lowest peak deceleration, but the highest integrated heat load.

2) The trajectory with the steepest flight-path angle that meets the exit energy constraint (lift-up) which results in the highest peak heating rate and the highest peak deceleration, but the lowest integrated heat load.

3) The trajectory whose flight-path angle results in the specified peak deceleration limit with a lift-up entry (5g) is achieved by a vehicle which flies lift-up until peak deceleration, and after the limit is reached, uses bank angle control to achieve the desired exit energy. The five Earth-g limit was assumed to be the maximum tolerable deceleration for short periods by a crew of deconditioned astronauts [30].

Figure 19 shows acceptable entry flight-path angles for a vehicle with 100 t entry mass, diameter of 15 m, and a lift-to-drag ratio (L/D) of 0.3. Note the significant increase assumed in aeroshell diameter relative to that discussed for the Mars robotic exploration program (factor of three). Even with this increased diameter, it is of interest to note that this aerocapture system has a β on the order of 400 kg/m^2 (more than 2.5 times that deemed possible by the robotic program and more than 4 times that proven on Mars to date).

The region of feasible trajectories is shaded in gray and is bounded by the constraints described previously. The theoretical entry corridor, without regard to deceleration limits, is the area between the lift-down and lift-up curves. This is the corridor achievable only with regard to the aerodynamics of the entry. When the deceleration limits of the crew are considered, the 5g lift-up curve provides the lower bound on the space for all entry velocities above approximately 6.5 km/s, narrowing the available corridor. The corridor width requirement is set by the approach navigation performance. Recent robotic Mars missions have demonstrated the ability to meet flight-path angle delivery requirements between ±0.25 and ±0.5 deg. For this study, a delivery accuracy requirement of ±0.5 deg was conservatively selected [30]. This total entry corridor width of 1 deg determines the maximum entry velocity feasible for a particular

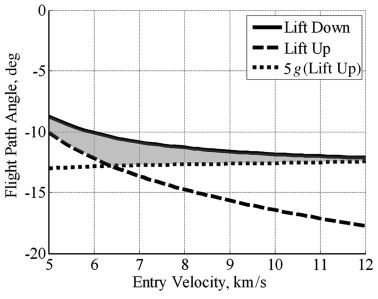

Fig. 19 Aerocapture corridor width as a function of Mars entry velocity for $L/D = 0.3$.

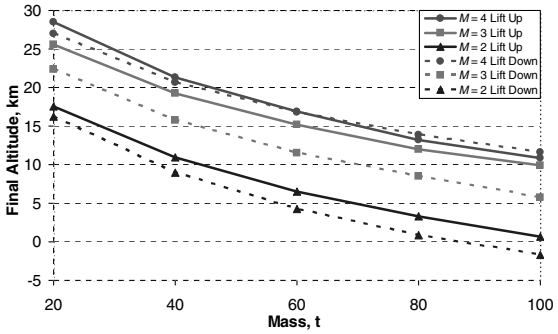

Fig. 20 Transition altitude as function of entry mass for a 15-m-diam aeroshell with $L/D = 0.3$.

vehicle configuration. From Fig. 19, an aerocapture $L/D = 0.3$ is sufficient (for an entry flight-path angle requirement of ± 0.5 deg) for Mars entry velocities under 9.1 km/s, a likely condition for most human Mars exploration architectures. Following aerocapture, the vehicle performs a small periapsis raise maneuver to insert into a parking orbit.

B. Entry from Orbit

Once orbital operations are complete, the Mars crew initiates an entry-from-orbit sequence. A parametric study of entry-from-orbit trajectories was performed for vehicles of a scale suitable for human missions [28]. Figure 20 depicts the altitudes at which the vehicle has slowed to various supersonic conditions for a range of potential entry masses, assuming a vehicle with $L/D = 0.3$ and 15 m diam entering from orbit. These curves were used to assess where in the EDL profile to transition from hypersonic entry to supersonic deceleration via parachutes or propulsive descent. Figure 20 highlights how difficult it is to slow a human-scale vehicle with high ballistic coefficient (entry mass of 50–100 t) before impact with the surface due to the low-density Mars atmosphere.

As shown in Fig. 20, the initial conditions for the supersonic descent segment are strongly dependent on ballistic coefficient (entry mass). For a 15-m-diam aeroshell and 60 t entry mass, the vehicle reaches Mach 2 at 5 km altitude, about the minimum possible from a descent timeline perspective. However, a 100 t vehicle packaged within a 15-m-diam aeroshell does not reach Mach 2 until it is at the surface. Note that a Mach 3 aerodynamic decelerator may allow use of a 100 t entry system for human Mars exploration. In addition, the heavy dependence on ballistic coefficient tends to favor larger aeroshells, and aerodynamic shapes that have a high drag coefficient, with only modest impact on landing site elevation capability as a result of lift performance. As shown in Fig. 20, lift can increase the terminal entry altitude by 3–5 km (difference between the lift-up and lift-down entries).

C. Aeroshell Shape and Size

A 70 deg sphere-cone forebody (see Fig. 21) was assumed for this 15-m-diam aeroshell because its geometry is traceable to the Viking and subsequent robotic landers and this forebody shape provides a relatively high hypersonic drag coefficient. In this respect, capsules and other blunt shapes compare favorably to slender-body designs that offer lift and higher L/D at the expense of drag (and therefore final altitude). When flown at an $L/D = 0.3$, this configuration provides a greater than 1 deg wide entry corridor for aerocapture velocities up to 9.1 km/s, with stagnation point peak heating rates on the order of 400 W/cm^2 and maximum decelerations in the range of 3–5 Earth-g. In the entry-from-orbit mode, this configuration could provide the high drag necessary ($C_D = 1.40, \alpha = 20$ deg) to give the vehicle sufficient altitude at Mach 3 or 4 to perform the subsequent descent and landing events for entry masses in the range of 80–120 t. Note once again that this system has a β of 300–450 kg/m^2 (a factor of 3–4 higher than any vehicle flown to date in the robotic Mars exploration program).

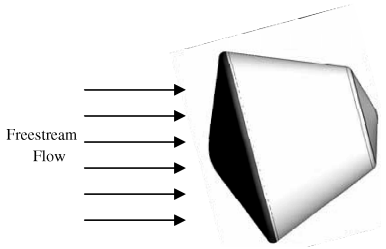

Fig. 21 70 deg sphere-cone aeroshell with $L/D = 0.3$ ($\alpha = 20$ deg, $C_D = 1.40$).

From a vehicle packaging standpoint, a large blunt body design is flexible. The diameter is driven to 15 m by the need to accommodate high-volume components such as the surface habitat and descent stage [30]. The capsule shape allows a large portion of the mass to be packaged near the front of the vehicle for improved hypersonic stability. The stability ratio (aft distance of center of mass divided by diameter) achieved for the packaged configuration was less than 0.35 (slightly less stable than current robotic designs). Because the lander is likely to transition to propulsive descent around Mach 3, aerodynamic stability problems at low supersonic Mach numbers are minimized.

The blunt body design also benefits from the fact that no vehicle reorientation is required during the EDL profile. In all flight regimes, acceleration is imparted to the vehicle in the same direction, thus facilitating the design of crew positions with respect to g-tolerance. In addition, no timeline is lost during the late stages of the EDL sequence to reorient the vehicle in preparation for propulsive descent. Mass estimation for such a system is described in [31]

Perhaps the largest EDL-imposed technical challenge inherent in such a mission architecture is the need for a heavy lift launch vehicle capable of lofting a 15-m-diam payload in one piece. Ultimately, this challenge must be weighed against the difficulty of launching a human-rated aeroshell in several pieces and then assembling and certifying it in low Earth orbit, developing inflatable/deployable aeroshell technology, or limiting the Mars exploration architecture to much smaller diameters and entry masses (through a surface rendezvous and assembly strategy).

D. Aerothermal Design

Aerocapture and entry from Mars orbit produce very different aerothermal environments. The aerocapture peak heating rate for an 8.5 km/s arrival velocity is about 20 times higher than the peak heating rate for a 4 km/s entry from orbit and the total integrated heat load is four times higher. As a result, the thermal protection system (TPS) required for the two maneuvers is quite different.

The aeroshell TPS may be configurable for dual-use (aerocapture and EDL). In this case, the same aeroshell is used first for aerocapture, and later for entry. Three concerns arise from this approach. First, because the TPS must be sized for the harsher aerocapture environment, the vehicle performs its entry-from-orbit with a more massive, high ballistic coefficient heat shield than would nominally be required, exacerbating heating and deceleration concerns. This also depresses the altitude where the vehicle has slowed to its Mach 3 or 4 transition altitude. Second, following the aerocapture maneuver, if the vehicle does not jettison the aerocapture heat shield, it must be designed to withstand a large amount of heat soaking back into the vehicle structure from the TPS. Extreme temperature cycles pose a structural design concern due to thermal expansion. Finally, a third challenge to a common aerocapture and entry TPS is the need to support the orbital functionality of a large crewed spacecraft without compromising the thermal protection system integrity for subsequent atmospheric maneuvers. Power, thermal, orbit-trim propulsion, attitude control, communications, and other spacecraft functions must be achieved from within the confines of the aeroshell, which implies that the backshell (and possibly the forebody) of the vehicle must allow openings for items such as solar arrays, radiators, engines, thrusters, and antenna.

An alternate approach for the TPS configuration would be to use separate, nested heat shields for aerocapture and EDL. This provides

the benefit of jettisoning the hot aerocapture TPS immediately following the aerocapture maneuver, and allows the use of much lighter TPS for entry, thus minimizing the vehicle's ballistic coefficient for that maneuver. The disadvantage of this approach is that packaging two nested heat shields on the vehicle requires a means of securing the primary heat shield to the structure and separating it without damaging the secondary heat shield, and likely results in an overall mass penalty. Additional work is required to assess these TPS configuration and mission operations options.

E. Supersonic Propulsive Descent

Following hypersonic entry, a vehicle intending to land on the surface of Mars must slow itself from supersonic velocities to a speed appropriate for a soft landing. This last deceleration phase, which involves only a few percent of the vehicle's remaining kinetic energy, has been initiated in past robotic missions below Mach 2.1 using some combination of parachutes and rocket-propelled descent. From Fig. 20, it is clear that Mach 2 initiation of this phase may not be sufficient for the high-mass entry systems associated with human exploration. The total descent time from Mach 3 or 4 to landing is on the order of 2 min. During this phase, several vehicle configuration changes are required. In a matter of seconds, the vehicle will need to reorient itself, an aeroshell and/or back shell may be jettisoned, parachutes may deploy, engines may start, navigation and hazard avoidance sensors must operate, and landing gear may deploy. In this very dynamic phase of flight, robust event sequencing and timeline margin are critically important.

To date, all parachutes used in the robotic Mars exploration program have been derived from the technology effort that led to the Viking flight project. These systems have been limited to diameters on the order of 10–20 m and supersonic deployments below Mach 2.1. As discussed in Sec. V, in an effort to improve landed mass, the robotic exploration program may pursue a large diameter supersonic parachute, likely no larger than 30 m and deployed at velocities below Mach 2.7 (in response to thermal constraints). As a result of the large masses involved, parachutes sized for human exploration systems would represent a significant departure (in both size and deployment Mach number) from their robotic counterparts. In addition, due to their size, such systems will require significant opening times. For example, to decelerate a 100 t vehicle from Mach 3 conditions to 50 m/s near the Mars surface would require a supersonic parachute diameter on the order of 130 m. Similarly, a 50 t vehicle requires a supersonic parachute diameter on the order of 90 m. Although clustered supersonic chutes are an option, the size of such systems would still result in large timeline penalties for opening. As such, a parachute descent phase for Mars human exploration vehicles, similar to the concepts now used for robotic landers, is likely impractical.

Drogue parachutes (of similar diameter to the main chutes employed by the robotic program) may still be necessary to stabilize a vehicle supersonically or effect separation events, but the effect of a large vehicle disrupting the flow in front of the parachute cannot be neglected because the size of the vehicle (15 m diam) may be on the same order as the size of its parachute. Flow interactions around the parachute will be complicated further if drogue stabilization is required during propulsive descent. This possibility may arise if the descent engines, being clustered under the vehicle center of mass, lack sufficient moment arm to overcome aerodynamic torques at supersonic conditions.

Propulsive descent requirements were evaluated based on a gravity turn maneuver initiated at Mach 4, 3, or 2. The results included the ΔV, thrust-to-weight, and propellant mass fraction requirements. A 265 m/s allowance was made for a crossrange maneuver associated with landing next to a preemplaced asset without endangering it. Items varied in this trade study include vehicle mass, vehicle diameter, and whether or not the aeroshell was released before propulsive initiation. The trajectory flown was a simple constant-thrust gravity turn, followed by a lower-thrust terminal descent and landing. No attempt was made to find a more fuel-optimal descent profile, because other unmodeled considerations (e.g., range safety and landing redesignation) will contribute significantly to the propellant situation.

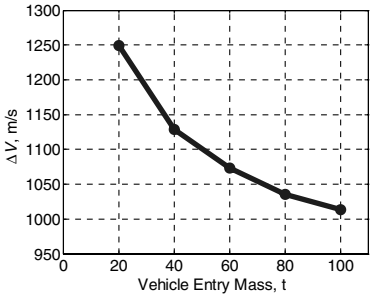

Fig. 22 ΔV for propulsive descent from Mach 3.

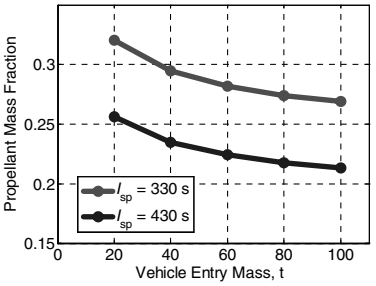

Fig. 23 Propellant mass fraction for propulsive descent from Mach 3.

Figure 22 shows that propulsive descent from Mach 3 requires 1.0–1.25 km/s of velocity change, including the 265 m/s cross range maneuver. This figure shows that ballistic coefficient, although not a dominant factor, does play a role. A lower ballistic coefficient leads to very low thrust-to-weight ratios (<0.5), longer flight times, higher gravity losses, and therefore a somewhat higher cumulative ΔV.

Figure 23 shows the propellant mass fraction (propellant mass/entry mass) required of a large Mars lander for two different values of specific impulse. Mass fractions typically fall in the range of 20–30%, for the propulsive deceleration and the 265 m/s cross range maneuver. Raising the specific impulse by 100 s lowered the propellant mass fraction by 5–7%. Although an all-propulsive solution for decelerating from Mach 3 to landing requires a relatively large amount of propellant, it has the advantage of being insensitive to atmospheric uncertainty and to landing site altitude.

Whereas parachutes alone must be unreasonably large when sized to decelerate large payloads at Mars, the all-propulsive solution results in high propellant mass fractions and requires aeroshell separation and propulsive descent initiation to take place at supersonic speeds. As such, a trade study was conducted to quantify how a large, supersonic parachute coupled with propulsive descent could mitigate these issues. In this assessment, aggressive assumptions were made in regard to parachute deployment conditions (Mach 3) and altitude requirements for the subsequent descent and landing events. Figure 24 shows the parachute sizes required to decelerate a payload from Mach 3 to Mach 0.8 at an

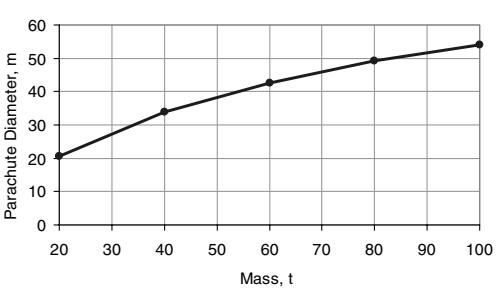

Fig. 24 Parachute diameter as function of entry mass for Mach 3 to Mach 0.8 deceleration.

altitude of 2 km. A Mach number of 0.8 (approximately 180 m/s) was chosen to mitigate the aeroshell separation and recontact concerns of current robotic landers. Figure 24 shows that a 30 m, Mach 3 parachute allows for a subsonic propulsive deceleration maneuver if entry masses are below approximately 33 t. This same parachute can slow the vehicle to Mach 1 at 2 km for entry masses less than 50 t. For entry masses above 50 t, a larger chute is required (with a significant opening time penalty), or the propulsive deceleration maneuver must begin supersonically.

An additional benefit of this approach is that the parachute can be used to separate the payload from the aeroshell. Atmospheric uncertainty is a major driver for parachute-assisted descent. The results described previously are for a nominal atmosphere. If a conservative density is modeled, the 30 m parachute is only practical for entry masses below approximately 20 t. Parachute-assisted propulsive descent still requires significant propellant mass fraction to bring the vehicle from Mach 0.8 to a soft landing. Overall, the total propellant mass fraction required for descent and landing will decrease from 20–30% of entry mass for an all-propulsive system (see Fig. 23), to a range of 12–18% for a parachute-assisted system.

Additional work is required to determine a feasible approach to transition from an entry to landing configuration supersonically. For the large mass entry systems associated with human Mars exploration, this transition is likely to be initiated at Mach 3 or 4. For this reason and due to extreme size requirements, parachute systems similar to the concepts now in use by robotic systems, are likely impractical, even when coupled with subsequent propulsive deceleration. Options for further study include large aerodynamic decelerators with robust functionality from Mach 3 or 4 to the surface and propulsive descent systems that are initiated supersonically.

F. Pinpoint Landing and No-Fly Zones

A human exploration landing system will require pinpoint landing capability (within 100 m, 3-σ), both for mission safety, given the extreme variability of the Mars surface, and to ensure rendezvous with predeployed exploration assets. In meeting these objectives, the human exploration entry system must approach the landing site on a trajectory that does not discard debris created during the EDL sequence (e.g., separated stages) upon the existing surface assets. In a Mars outpost strategy, most of these same requirements must be met by earlier robotic missions.

As discussed in Sec. IV, with use of a low L/D aeroshell, an autonomous atmospheric guidance algorithm, and an accurate IMU, the vehicle's position knowledge error at parachute deployment can effectively be reduced to the navigation knowledge error at IMU initialization. Landed position error can be reduced below that demonstrated and planned in the current robotic program by obtaining surface imagery and performing comparison with onboard maps to determine surface-relative position. Propulsion may then be used to achieve terrain-relative landed accuracies within 100 m of the target [25].

VII. Conclusions

The United States has successfully landed five robotic systems on the surface of Mars. These systems all had landed mass below 0.6 t, had landed footprints on the order of hundreds of km, and landed at sites below −1.4 km MOLA elevation due the need to perform entry, descent, and landing operations in an environment with sufficient atmospheric density. Robotic exploration systems engineers are struggling with the challenges of increasing landed mass capability to 1 t, while improving landed accuracy to tens of kilometers and landing at a site as high as +2 km MOLA elevation. Subsequent robotic exploration missions under consideration for the 2010 decade may require a doubling of this landed mass capability. To date, no credible Mars EDL architecture has been put forward that can safely place a 2 t payload at high elevations on the surface of Mars at close proximity to scientifically interesting terrain. This difficulty is largely due to the Mars program's continued reliance on Viking-era space qualification technology.

In this investigation, the technology challenges associated with improving our landing site access and landed mass capability were reviewed. Approaches being investigated by the robotic Mars exploration program to increase landed mass capability to 1 t, while improving landed accuracy to tens of kilometers and landing at a site as high as +2 km MOLA elevation were described, and it was shown that this class of mission may be the limit for the Viking-era EDL technology, which has served us so well. EDL technology challenges emanate from 1) a Mars atmosphere, with significant variability, that is thick enough to create substantial heating, but not sufficiently low terminal descent velocity; 2) a Mars surface environment of complex rocks, craters, dust, and terrain patterns; and 3) the high cost of replicating a Mars-relevant environment for space flight qualification of new EDL technologies. Robotic exploration technology options that may greatly improve current EDL system delivery limits include larger diameter parachutes that deploy at Mach numbers as high as 2.7, inflatable/deployable aerodynamic decelerators that greatly reduce ballistic coefficient, and pinpoint landing technologies focused on robust terrain-relative navigation.

This investigation also presented a potential entry, descent, and landing sequence for Mars human exploration, highlighting the technology and systems advances required. Unfortunately, it is concluded that Mars human exploration aerocapture and EDL systems will have little in common with current and next-decade robotic systems. As such, significant EDL technology and engineering investment is required to achieve the capabilities required for a human mission to Mars. Additional refinement is required in the following human exploration EDL architectural areas: 1) assessment of aerocapture/entry TPS configuration options, and 2) an approach to efficiently transition from the entry to landing configuration at supersonic conditions within stringent timeline constraints. For the large mass entry systems associated with human Mars exploration, this transition is likely to be initiated at Mach 3 or 4. For this reason and due to extreme size requirements, parachute systems similar to the concepts now in use by the robotic exploration program are likely impractical. EDL technology options for further study include large aerodynamic decelerators deployed for hypersonic and/or supersonic flight, propulsive descent systems that are initiated supersonically, and pinpoint landing systems focused on robust terrain-relative navigation.

Acknowledgments

A portion of the research described in this paper was carried out at the Jet Propulsion Laboratory, California Institute of Technology, under a contract with the National Aeronautics and Space Administration. The authors are indebted to the following personnel for helpful discussions and insight in the preparation of this material: Mark Adler, Adam Steltzner, Allen Chen, and Robert Mitcheltree of the Jet Propulsion Laboratory; Juan Cruz and John Dec of the NASA Langley Research Center; Al Witkowski of Pioneer Aerospace; Grant Wells, Amanda Verges, and Jarret Lafleur of the Georgia Institute of Technology; and Clem Tillier of the Charles Stark Draper Laboratory.

References

[1] Manning, R., and Adler, M., "Landing on Mars," *AIAA Space 2005 Conference, Long Beach, CA*, AIAA Paper 2005-6742, Sept. 2005.

[2] Steltzner, A., "Mars Science Laboratory Entry, Descent and Landing System," *2006 IEEE Aerospace Conference, Big Sky, MT*, Inst. of Electrical and Electronics Engineers Paper 1497, March 2006.

[3] Way, D., Powell, R., Chen, A., and Steltzner, A., "Sensitivity Analysis of Design Parameters Affecting the Mars Science Laboratory Entry, Descent, and Landing System Altitude Performance and Timeline Margin," *2006 IEEE Aerospace Conference, Big Sky, MT*, Inst. of Electrical and Electronics Engineers Paper 1465, March 2006.

[4] Bernard, D., and Golombek, M., "Crater and Rock Hazard Modeling for Mars Landing," *AIAA Space 2001 Conference and Exposition, Albuquerque, NM*, AIAA Paper 2001-4697, Aug. 2001.

[5] Golombek, M., and Rapp, D., "Size-Frequency Distributions of Rocks on Mars and Earth Analog Sites: Implications for Future Landed Missions," *Journal of Geophysical Research*, Vol. 102, No. E2,

Feb. 1997, pp. 4117–4129.
[6] Golombek, M., Haldemann, A., Forsberg-Taylor, N., DiMaggio, E., Schroeder, R., Jakosky, B., Mellon, M., and Matijevic, J., "Rock Size-Frequency Distributions on Mars and Implications for Mars Exploration Rover Landing Safety and Operations," *Journal of Geophysical Research*, Vol. 108, No. E12, 2003, p. 8086.
[7] Kirk, R., Howington-Kraus, E., Redding, B., Galuszka, D., Hare, T., Archinal, B., Soderblom, L., and Barrett, J., "High-Resolution Topomapping of Candidate MER Landing Sites with Mars Orbiter Camera Narrow-Angle Images," *Journal of Geophysical Research*, Vol. 108, No. E12, 2003, p. 8088.
[8] Pohlen, J., Maytum, B., Ramsey, I., and Blanchard, U. J., "Evolution of the Viking Landing Gear," Jet Propulsion Lab. TM 33-777, Pasadena, CA, 1977.
[9] Spencer, D., Blanchard, R., Braun, R., Kallemeyn, P., and Thurman, S., "Mars Pathfinder Entry, Descent, and Landing Reconstruction," *Journal of Spacecraft & Rockets*, Vol. 36, No. 3, 1999, pp. 357–366.
[10] Desai, P., and Knocke, P., "Mars Exploration Rovers Entry, Descent, and Landing Trajectory Analysis," *AIAA/AAS Astrodynamics Specialist Conference and Exhibit*, AIAA, Reston, VA, 2004.
[11] Steltzner, A., Lee, W., Bruno, R., and Desai, P., "Mars Exploration Rovers Entry, Descent, and Landing Phase and the Use of Aerodynamic Decelerators," *17th AIAA Aerodynamic Decelerator Systems Technology*, AIAA Paper 2003-212, Reston, VA, May 2003.
[12] Shotwell, R.,, "Phoenix: The First Mars Scout Mission," *55th International Astronautical Congress, Victoria, British Columbia*, International Astronautical Federation Paper 04-IAF-Q.3.B.03, Oct. 2004.
[13] Rivellini, T., "Challenges of Landing on Mars," *Frontiers of Engineering: Reports on Leading-Edge Engineering from the 2004 NAE Symposium on Frontiers of Engineering*, Vol. 34, No. 4, 2005, pp. 23–32.
[14] Wright, M., Edquist, K., Hollis, B., Olejniczak, J., and Venkatapathy, E., "Status of Aerothermal Modeling for Current and Future Mars Exploration Missions," *2006 IEEE Aerospace Conference, Big Sky, MT*, Inst. of Electrical and Electronics Engineers Paper 428, March 2006.
[15] Edquist, K., "Afterbody Heating Predictions for a Mars Science Laboratory Entry Vehicle," *38th AIAA Thermophysics Conference, Toronto, Ontario, Canada*, AIAA Paper 2005-4817, June 2005.
[16] Gillis, C., "Viking Decelerator System: An Overview," AIAA Paper 73-442, 1973.
[17] Witkowski, A., and Brown, G., "Mars Deployable Decelerators Capability Roadmap Summary," *2006 IEEE Aerospace Conference, Big Sky, MT*, Inst. of Electrical and Electronics Engineers, Paper 1585, March 2006.
[18] Cruz, J., Mineck, R., Keller, D., and Bobskill, M., "Wind Tunnel Testing of Various Disk-Gap-Band Parachutes," *17th AIAA Aerodynamics Decelerator Systems Technology Conference, Phoenix, AZ*, AIAA Paper 2003-2129, May 2003.
[19] Witkowski, A., Kandis, K., Bruno, R., and Cruz, J., "Mars Exploration Rover Parachute System Performance," *18th AIAA Aerodynamic Decelerator Systems Technology Conference, Munich, Germany*, AIAA Paper 2005-1605, May 2005.
[20] Cruz, J., Cianciolo, A., Powell, R., Simonsen, L., and Tolson, R., "Entry, Descent and Landing Technology Concept Trade Study for Increasing Payload Mass to the Surface of Mars," *Proceedings of the 4th International Symposium on Atmospheric Reentry Vehicles and Systems, Arachon, France*, Association Aeronautique et Astronautique de France, March 2005.
[21] Mitcheltree, R., Bruno, R., Slimko, E., Baffes, C., and Konefat, E., "High Altitude Test Program for a Mars Subsonic Parachute," *18th AIAA Aerodynamic Decelerator Conference, Munich, Germany*, AIAA Paper 2005-1659, May 2005.
[22] Witkowski, A., Machalick, A., and Taeger, Y., "Mars Subsonic Parachute Technology Task System Overview," *18th AIAA Aerodynamic Decelerator Conference, Munich, Germany*, AIAA Paper 2005-1657, May 2005.
[23] Knocke, P. C., Wawrzyniak, G., Kennedy, B., Desai, P., Parker, T., Golombek, M., Duxbury, T., and Kass, D., "Mars Exploration Rover Landing Dispersion Analysis," *2004 AIAA Astrodynamics Conference*, AIAA Paper 2004-5093, Aug. 2004.
[24] Braun, R., Powell, R., Cheatwood, F., Spencer, D., and Mase, R., "Mars Surveyor 2001 Lander: A First Step Toward Precision Landing," *49th International Astronautical Congress, Melbourne, Australia*, International Astronautical Federation Paper 98-Q.3.03, Sept. 1998.
[25] Wolf, A., Tooley, J., Ploen, S., Gromov, K., Ivanov, M., and Acikmese, B., "Performance Trades for Mars Pinpoint Landing," *2006 IEEE Aerospace Conference, Big Sky, MT*, Inst. of Electrical and Electronics Engineers Paper 1661, March 2006.
[26] Rohrschneider, R., and Braun, R., "Survey of Ballute Technology for Aerocapture," *Journal of Spacecraft and Rockets* (to be published), 2007.
[27] Brown, G., Epp, C., Graves, C., Lingard, J., and Darly, M., "Hypercone Inflatable Supersonic Decelerator," AIAA Paper 2003-2167, 2003.
[28] Wells, G., Lafleur, J., Verges, A., Manyapu, K., Christian, J., Lewis, C., and Braun, R., "Entry, Descent and Landing Challenges of Human Mars Exploration," *29th AAS Guidance and Control Conference, Breckenridge, CO*, American Astronautical Society Paper 06-072, Feb. 2006.
[29] Hall, J., Noca, M., and Bailey, R., "Cost-Benefit Analysis of the Aerocapture Mission Set," *Journal of Spacecraft & Rockets*, Vol. 42, No. 2, 2005, pp. 309–320.
[30] Hofstetter, W., Wooster, P., Nadir, W., and Crawley, E., "Affordable Human Moon and Mars Exploration Through Hardware Commonality," *AIAA Space 2005 Conference, Long Beach, CA*, AIAA Paper 2005-6757, Sept. 2005.
[31] Christian, J., Manyapu, K., Wells, G., Lafleur, J., Verges, A., and Braun, R., "Sizing of an Engry, Descent, and Landing System for Human Mars Exploration," *AIAA Space 2006 Conference, San Jose, CA*, AIAA Paper 2006-7427, Sept. 2006.

D. Spencer
Associate Editor